

# Lightweight, Ultra-Wideband, and Polarization-Insensitive Metamaterial Absorber Using a Multilayer Dielectric Structure for C- and X-Band Applications

Duy Tung Phan, Thi Kim Thu Nguyen, Ngoc Hieu Nguyen, Dac Tuyen Le, Xuan Khuyen Bui, Dinh Lam Vu, Chi Lam Truong, and Thi Quynh Hoa Nguyen\*

The design of a lightweight and ultra-wideband absorber for C and X bands is still a challenge as the dimension of the absorber is relatively large in such a relatively low-frequency band. Herein, an ultra-wideband and lightweight metamaterial absorber (MMA) is presented for C- and X-band applications. The unit cell of the proposed MMA consists of four copper sectors loaded by lumped resistors and a continuous copper ground plane, which is printed on two FR-4 substrates. Furthermore, an airgap separating the FR-4 layers is used as the active substrate medium of the MMA to achieve both ultra-wideband absorption spectra and lightweight design. The MMA is investigated by simulation and measurement, showing that a good agreement is achieved. The result indicates that the absorptivity of the MMA under both transverse electric (TE) and transverse magnetic (TM) polarizations is greater than 90% in a wide range from 3.7 to 13.6 GHz for all polarization angles. Compared to other reported broadband absorbers, the proposed MMA shows an ultra-wide absorption bandwidth and a lightweight design, which demonstrates a great potential for C-and X-band applications.

## 1. Introduction

Nowadays, microwave absorbers are a fast-growing field with applications in both military and consumer electronics to reduce electromagnetic (EM) interference among microwave components or electronic circuits mounted on the same platform.<sup>[1,2]</sup> Conventionally, the traditional absorbing materials are divided into two categories, including filling type using lossy fillers and structure design type using resistance sheets.<sup>[3,4]</sup> Recently, microwave metamaterial absorbers (MMAs), which are composed of subwavelength periodic patterns and dielectric substrates, have been attracting extensive interest due to their excellent design ability.<sup>[5–15]</sup> By controlling the dimensions of the electric and magnetic components, the permittivity and permeability of metamaterials can be varied and the impedance of MMAs can

be matched to free space. Therefore, perfect absorption can be obtained by theoretical prediction. The perfect MMA was first experimentally developed by Landy et al. in the microwave region<sup>[6]</sup> and followed by a variety of applications such as subwavelength imaging,<sup>[1]</sup> energy harvesting,<sup>[2]</sup> and sensing.<sup>[5]</sup> Compared to the traditional absorber, MMAs can give some advantages, such as the thickness of the MMA being much thinner than that of the traditional absorber and the fabrication cost of MMA being lower.<sup>[16–19]</sup>

However, most of the existing MMA designs have a narrow bandwidth due to these resonance features, thus limiting practical applications that require a wide bandwidth. Therefore, some methods for enlarging the absorption bandwidth of MMAs have been developed, such as using multiple layers of metal-dielectric stacks<sup>[20,21]</sup> and combining various unit-cell sizes.<sup>[22]</sup> These methods have drawbacks such as fabrication process complexity and limitation of the absorption bandwidth. Recently, broadband MMAs have successfully been designed based on materials with low- $Q$ -factor profiles, for example, a conductive polymer,<sup>[23]</sup> indium tin oxide,<sup>[24]</sup> and resistive ink.<sup>[25]</sup> However, the achieved absorption spectra of the above MMAs are relatively narrow (<80%). Furthermore, all-dielectric layers<sup>[26]</sup> and water-based<sup>[18,27,28]</sup> methods have been developed to achieve broadband EM-absorbing metastructures. However, a thicker insulator


D. T. Phan, T. K. T. Nguyen, Dr. N. H. Nguyen, Prof. T. Q. H. Nguyen  
School of Engineering and Technology  
Vinh University  
182 Le Duan, Vinh city, Vietnam  
E-mail: ntqhoa@vinhuni.edu.vn

Prof. D. T. Le  
Department of Physics  
Hanoi University of Mining and Geology  
18 Pho Vien, Hanoi, Vietnam

Dr. X. K. Bui  
Institute of Materials Science  
Vietnam Academy of Science and Technology  
18 Hoang Quoc Viet, Cau Giay, Hanoi, Vietnam

Prof. D. L. Vu  
Graduate University of Science and Technology  
Vietnam Academy of Science and Technology  
18 Hoang Quoc Viet, Cau Giay, Hanoi, Vietnam

C. L. Truong  
NTT Hi-Tech Institute  
Nguyen Tat Thanh University  
Ho Chi Minh City, Vietnam

 The ORCID identification number(s) for the author(s) of this article can be found under <https://doi.org/10.1002/pssb.202100175>.

DOI: 10.1002/pssb.202100175

layer leads to heavy weight of the overall device, which limits its practical applications.

In this article, a lightweight, ultra-wideband, and polarization-insensitive absorber has been designed, fabricated, and experimentally measured. The MMA is composed of two FR-4 layers separated by an airgap forming a multilayer substrate structure. Furthermore, four chip resistors are properly integrated on the top layer of the MMA. By combining both ideas, the proposed MMA can achieve an ultra-wideband absorption spectrum within a lightweight design. The measured bandwidth with an absorptivity higher than 90% ranges from 3.7 to 13.6 GHz with a relative bandwidth of 114.5%, which entirely covers both the X and C bands. Furthermore, the proposed MMA has advantages of polarization insensitiveness and angle stability for both the transverse electric (TE) and transverse magnetic (TM) polarizations. Thus, this designed MMA promises a good candidate for various practical applications in the X and C bands.

## 2. Structure Design and Method

The proposed MMA consists of a periodic array of unit cells with a period ( $P$ ) of 13.6 mm. A schematic drawing of the unit cell is shown in **Figure 1**. The top and bottom layers of the unit cell are made of copper with an electric conductivity of  $5.96 \times 10^7 \text{ S m}^{-1}$  and a thickness ( $t$ ) of 0.035 mm. It should be noted that the bottom layer acts as the ground to eliminate the transmission. The dielectric layer consists of two identical FR-4 layers ( $\epsilon_1 = 4.3$ ,  $\tan\delta = 0.025$ ) separated by an airgap. It is well known that the design of a wideband absorber at a low frequency band (e.g., C band) requires a relatively large thickness of the dielectric layer. Therefore, our expectation of using the airgap is to achieve an ultrawide absorption bandwidth while maintaining the light weight of the MMA design. The thickness of the FR-4 layer and airgap is  $h$  and  $d$ , respectively (**Figure 1a**).

Our recent study showed that a broadband MMA structure based on a split circle ring (SCR) loaded with four lumped resistors exhibited broadband absorption with absorptivity above 90% in the frequency range 7.8–12.6 GHz.<sup>[29]</sup> However, this structure is insensitive to the incident angle when the incident angle is quite low (less than  $30^\circ$ ). Recently, the design of a metasurface utilizing the gradient structure was proposed to improve the

**Table 1.** Optimum parametric values of the unit cell of the MMA.

Parameter	$P$	$t$	$h$	$d$	$R$	$S$
Value (mm)	13.6	0.035	0.8	4.8	6.4	9.2

angle tolerance in a cross-polarization converter.<sup>[15]</sup> Therefore, in this study, to enhance the angle tolerance, the top metallic pattern is based on a gradient structure formed by a modified split circle ring, as displayed in **Figure 1b**. The top pattern of the proposed MMA is considered a frequency-selective surface (FSS). As shown in **Figure 1b**, the top layer of the unit cell consists of four copper sectors formed by a disk with a square-shaped hollow. The radius of the circle ( $R$ ) and edge of the hollow square ( $S$ ) are 6.4 and 9.2 mm, respectively. Moreover, four lumped resistors of  $180 \Omega$  are loaded on the top layer (between the sectors) to broaden the absorption bandwidth of the MMA fully cover the whole C and X band. The optimum dimensions of the MMA are listed in **Table 1**.

To analyze the absorption performance of the MMA, a numerical simulation based on the commercial computer simulation technology (CST) using a frequency-domain solver was performed. In this simulation setup, the periodic boundary conditions are chosen as the unit cell for the  $x$ - and  $y$ -directions, and the open boundary condition is set to the  $z$ -direction.

## 3. Results and Discussion

**Figure 2** shows the simulated absorption spectra of the proposed MMA under TE and TM polarizations. The proposed MMA with four chip resistors shows a high absorption rate above 90% in an ultra-wideband of 3.7 to 13.6 GHz for both TE and TM polarizations, which corresponds to the relative absorption bandwidth (RAB) of 114.5%. Furthermore, to evaluate the contribution of the chip resistors on the ultrawide absorption band characteristic of the proposed MMA, we also simulate the absorption spectra of the same MMA structure by removing the chip resistors loaded in the top layer. As shown in **Figure 2**, the MMA structure without chip resistors shows a very poor absorption performance in the band from 2 to 20 GHz. It is clear that the loading of chip

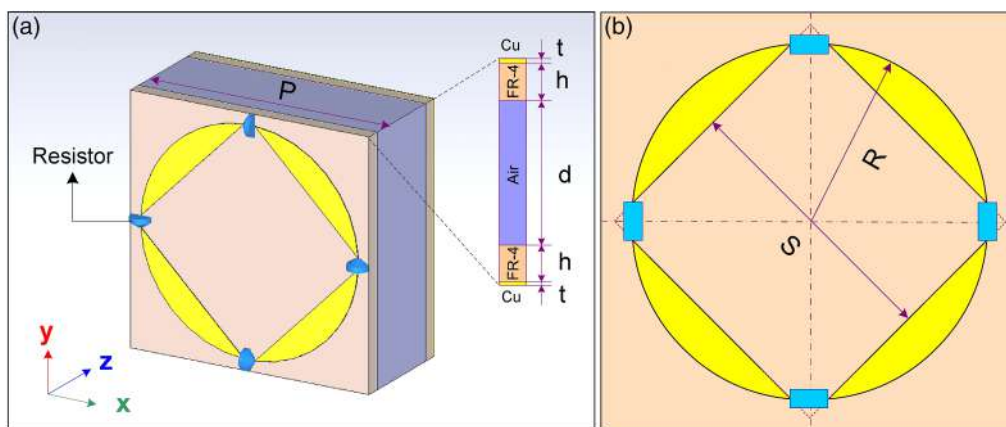


**Figure 1.** Schematic drawings of the designed unit cell with geometric: a) 3D view and b) top view.

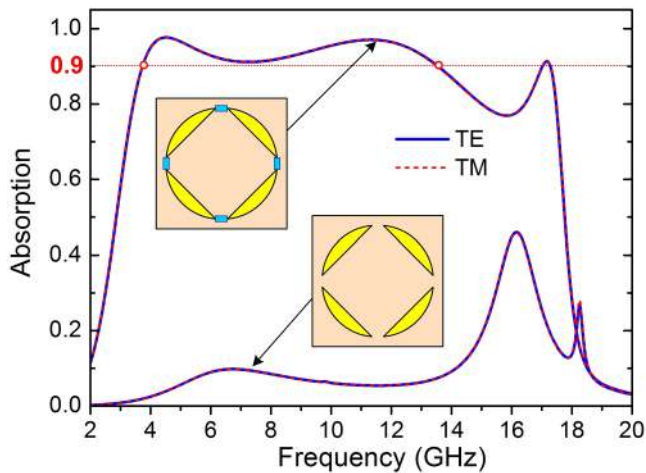


**Figure 2.** Absorption spectra of the designed MMA with and without chip resistors for TE and TM polarizations under normal incidence.

resistors on the FSS surface of the MMA plays an important role in obtaining the wideband impedance matching between the MMA and the free space, leading to improvement of the absorption rate as well as the absorption bandwidth of the MMA. It should be noted that the absorption band of the proposed MMA with chip resistors exhibits two distinct resonance absorption peaks at 4.5 and 11.4 GHz and entirely covers the X and C bands from 4 to 12 GHz.

Furthermore, simulation results for various oblique incidences of TE and TM polarization waves are shown in **Figure 3**. For

oblique incidences until  $\theta = 20^\circ$ , the absorption remains more than 90% for both TE and TM polarizations even though the bandwidth is very slightly decreased. We can observe from **Figure 3b** that the bandwidth of the MMA is rapidly decreased with the increase in the incident angle in the TM polarization because the direction of the magnetic field is parallel to the resistor surface.<sup>[30]</sup> For an incident angle of  $40^\circ$ , the absorption rate is maintained higher than 85% in the full X and C bands. On further increasing of the oblique incident angle up to  $60^\circ$ , the absorption intensity deteriorates but still persists above 70% in the X and C bands. **Figure 3c,d** shows the dependence of the incident angle on the absorption performance of the MMA for the TE and TM polarizations, respectively. This result confirms a high absorption level is still retained with a wide oblique incident angle, which is extremely interesting for a broadband absorber.

The polarization behavior of the MMA is also investigated, as shown in **Figure 4**. The simulated absorption spectra of the MMA under normal incidence for TE polarization are almost unchanged at different polarization angles. It proves that the proposed MMA exhibits a polarization-insensitive property because of its symmetry structure.

To gain insights into the contribution of the airgap layer to the broadband absorption characteristics of the proposed MMA, we study the absorption behavior of the MMA when the thickness of the airgap varies. Moreover, the physical explanation of the role of the airgap layer on the designed wideband MMA is also demonstrated using the equivalent circuit (EC) method. The EC of the unit cell is a series  $R, L, C$  in parallel with shorted transmission line sections as shown in **Figure 5**. The input

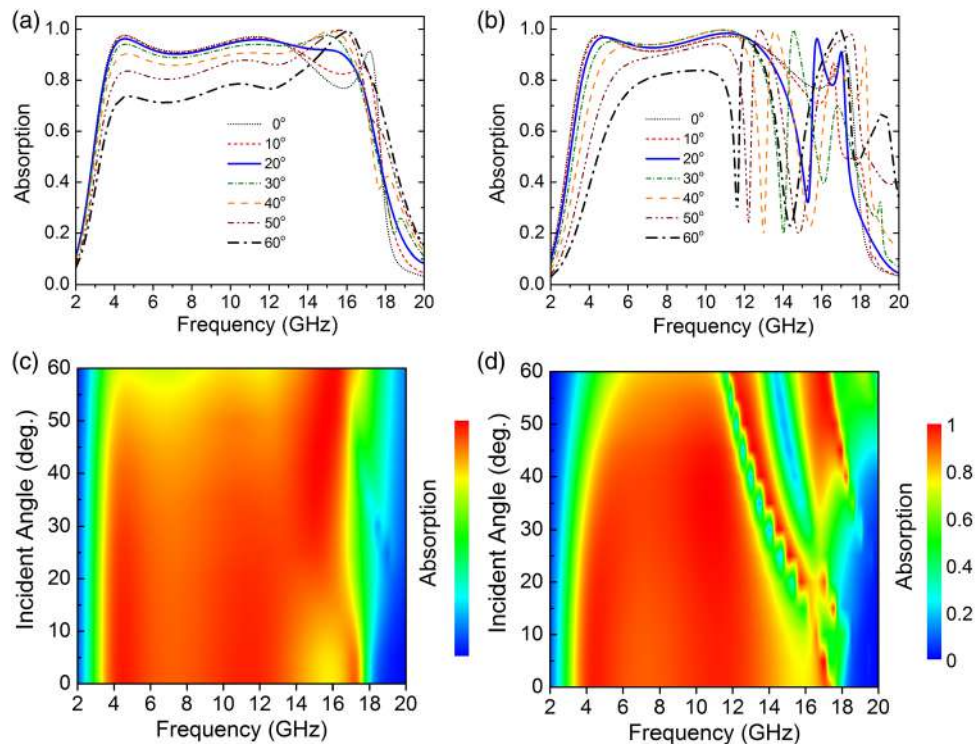


**Figure 3.** Absorption spectra of the proposed MMA with various incident angles of a,c) TE polarization and b,d) TM polarization.

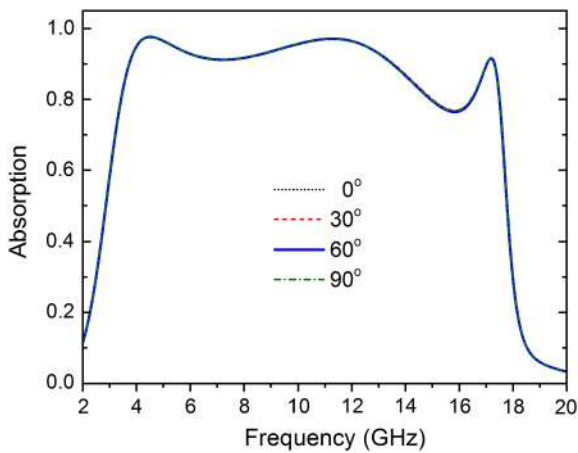


**Figure 4.** Absorption spectra of the proposed MMA with various polarization angles under normal incidence.

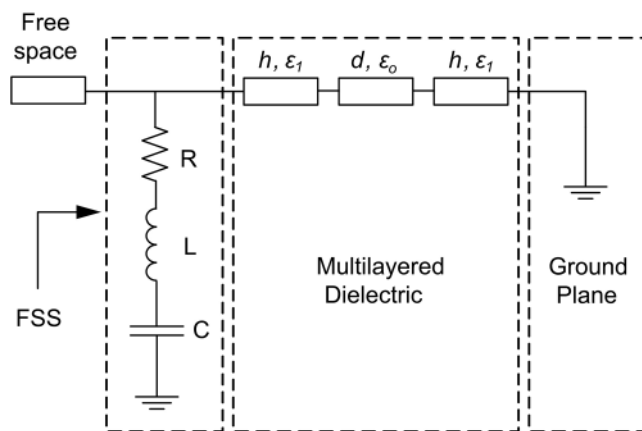


**Figure 5.** Equivalent circuit of a unit cell of the proposed MMA.

admittance of the MMA is equal to the parallel connection between the admittance of the FSS loaded chip resistors and the admittance of the dielectric slabs and airgap. The  $L$  and  $C$  parameters are determined by the shape of the FSS.<sup>[31]</sup> The

transmission line sections of thickness  $h$ ,  $d$ ,  $h$  denote the FR-4 substrate, airgap, and FR-4 substrate layers.

It is known that resonances can be created when the imaginary part of the input admittance equals zero.<sup>[32]</sup> When the length of a grounded dielectric slab is less than a half-wavelength, the susceptance of the FSS transitions from inductive to capacitive behavior as the frequency increases, whereas the trend is the opposite as the frequency increases when the length is greater than a half-wavelength.<sup>[32]</sup> When the thickness of the grounded dielectric slabs exceeds a quarter wavelength, the slabs behave as a capacitance.<sup>[31]</sup> The FSS's susceptance cancels out the susceptance of the short-circuited transmission line, which can be either inductive or capacitive, referring to the first and second resonances, respectively.<sup>[31–33]</sup> In this work, we fixed the thickness of the FR-4 substrate to 0.8 mm to obtain a lightweight design. Moreover, the size and shape of the FSS were also optimized and fixed to determine the  $L$  and  $C$ . Therefore, the thickness of the airgap can be used to control the resonant frequencies, while the real part of the input admittance contributed by the chip resistors affects the matching condition around resonances. With the fixed chip resistors of  $180 \Omega$  there is an optimized airgap thickness to create the resonances that exhibit the widest impedance matching, resulting in obtaining the widest absorption bandwidth. To determine the optimum airgap thickness, a parametric study of airgap thickness was conducted, as shown in **Figure 6a**. Moreover, the corresponding average absorption of the MMA in the C and X bands (4–12 GHz) with different thicknesses of airgap is also shown in **Figure 6b**. As shown in **Figure 6a,b**, the absorber exhibits the best absorption performance at an airgap of 4.8 mm, making it the optimum airgap thickness for the MMA design. At the airgap thickness of 4.8 mm, the maximum value of the average absorption of the MMA in the C and X bands is 93.8%. It should be noted that at the optimum airgap, the total thickness of the multilayered substrate is 6.4 mm, corresponding to a quarter wavelength at 9.2 GHz. Therefore, the optimum value of the airgap is related to the condition of the original Salisbury screen.<sup>[31,33]</sup>

The absorption mechanism of the MMA design with airgap thickness of 4.8 mm was analyzed through calculation of the input impedance and electric field and investigation of surface current distributions. Generally, the absorption of an absorber ( $A$ ) is given by the formula  $A = 1 - |S_{11}|^2 - |S_{21}|^2$ , where  $S_{11}$

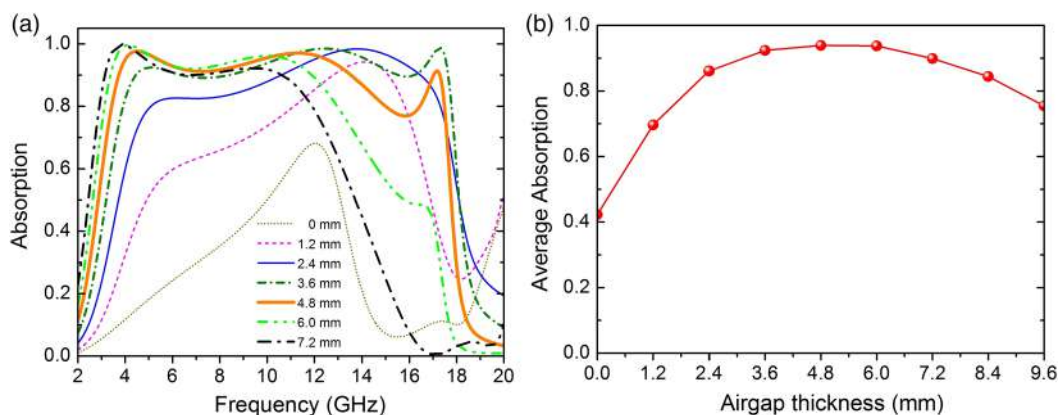


**Figure 6.** a) Absorption spectra of the proposed MMA and b) its average absorption with various different thicknesses of the airgap.



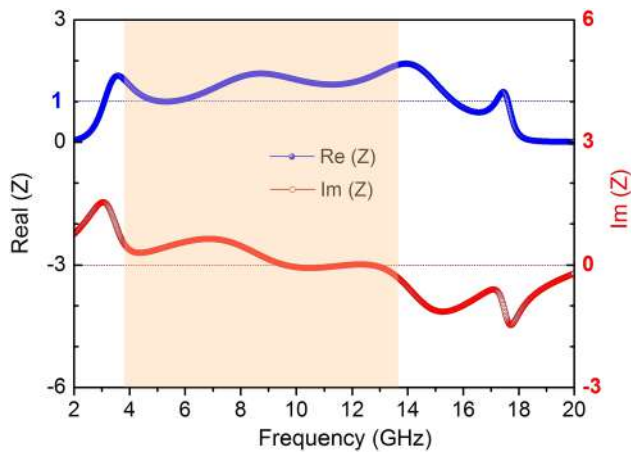


**Figure 7.** Normalized input impedance ( $Z$ ) of the proposed MMA versus frequency under normal incidence.

and  $S_{21}$  are the reflection and transmission coefficients. The bottom layer of the MMA is backed by a metallic layer, so no transmission occurs. Therefore, in this case,  $A = 1 - |S_{11}|^2$ .

When the impedance matching between the absorber structure and free space appears, the reflection becomes zero. Therefore, near-perfect absorption of the MMA can be achieved when impedance matching occurs. **Figure 7** shows the normalized input impedance ( $Z$ ) of the designed MMA, calculated based on the scattering parameter extraction.<sup>[34]</sup>

$$Z = \sqrt{\frac{(1 + S_{11})^2 - S_{21}^2}{(1 - S_{11})^2 - S_{21}^2}} = \frac{1 + S_{11}}{1 - S_{11}} \quad (1)$$

As shown in **Figure 7**, the real and imaginary components of the normalized impedance are close to 1 and 0, respectively, in the whole operating band range from 3.7 to 13.6 GHz. This observation confirms the good impedance matching between the MMA structure and free space in the wide frequency range, resulting in the obtaining of near-perfect broadband absorption response in this design.

**Figure 8a,b,c** shows the electric field distribution at different resonant frequencies of 4.5, 11.4, and 17.2 GHz. The electric field is concentrated at the inner corners of the proposed MMA sectors and lumped resistors. The concentrated electric field with high intensity on the lumped resistors can widen

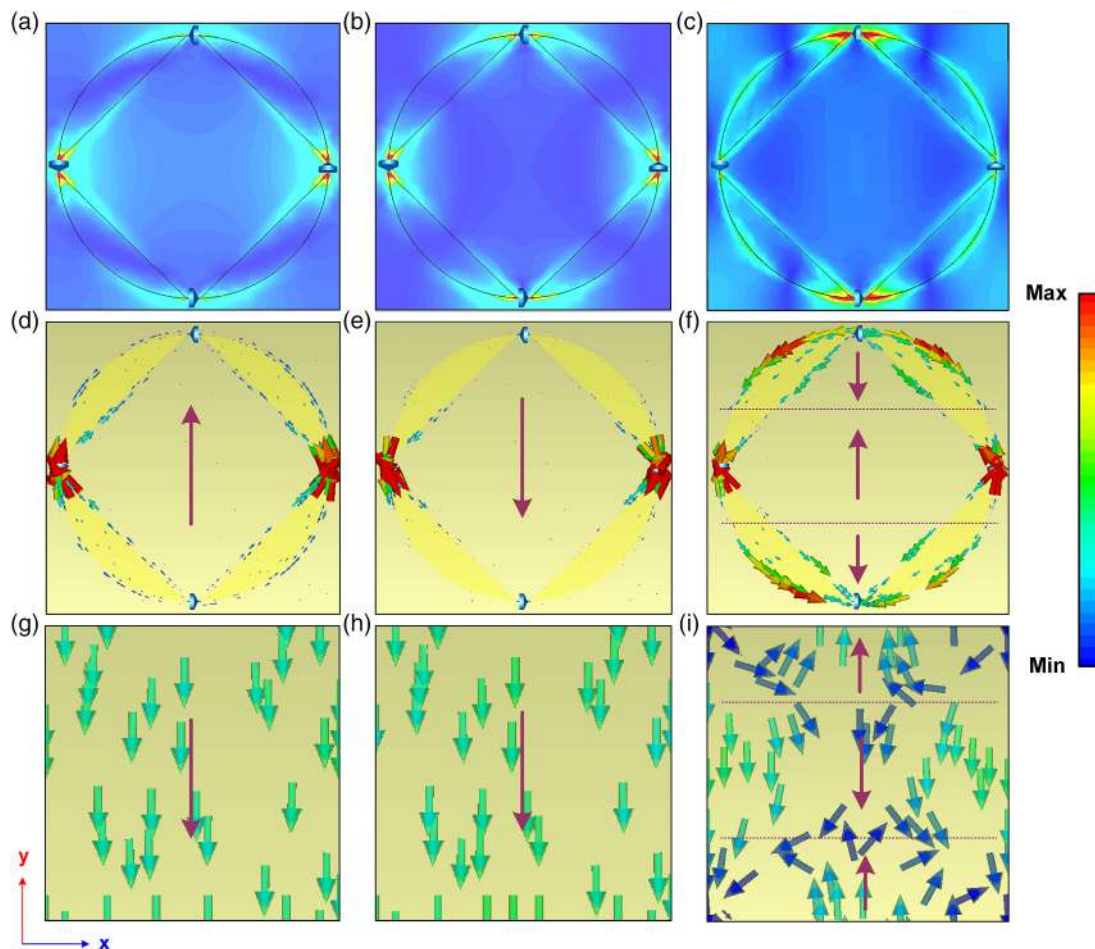


**Figure 8.** Distribution of a–c) the electric field and of the surface current on d–f) the top layer and g–i) the bottom layer of the proposed MMA at resonant frequencies of 4.5, 11.4, and 17.2 GHz, respectively.

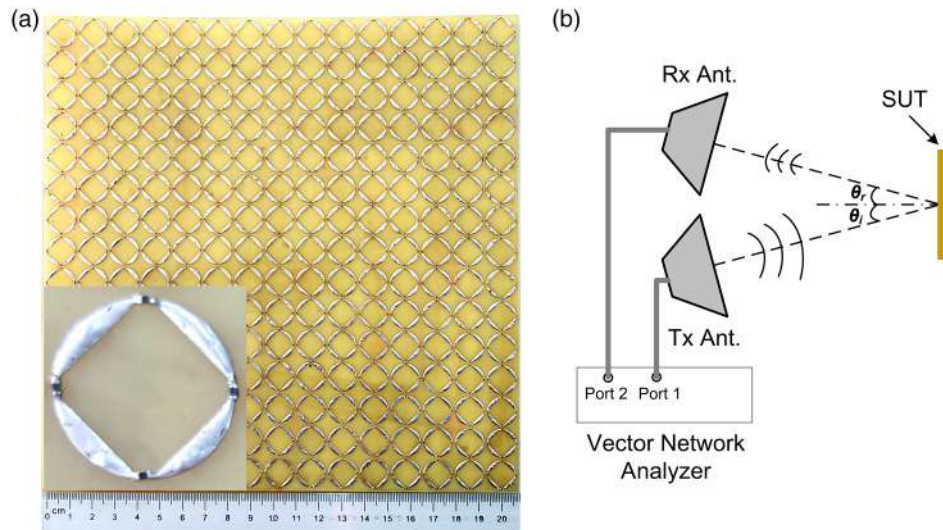


**Figure 9.** a) Fabricated MMA and b) schematic illustration of the measurement setup.

the absorption bandwidth.<sup>[29]</sup> The electric field distribution at the resonant frequencies of 4.5 and 12.7 GHz is mainly generated from the regions around the lumped resistors in the vertical axis and horizontal axis, respectively, while that at the resonant frequency of 11.4 GHz is formed from the regions in the vertical and horizontal axes. The direction of surface current on the top layer and bottom layer is antiparallel to each other at the lower resonant frequency of 4.5 GHz (Figure 8d,g), indicating that the perfect absorption at this resonant frequency is originated from the magnetic resonance. In contrast, at the resonant frequency of 11.4 GHz, the top and bottom surface currents are in the parallel direction (Figure 8e,h) and electric resonance is excited at this resonant frequency. However, at the higher frequency of 17.2 GHz, the top and bottom surface currents are separated into three distinct regions, with antiparallel currents in adjacent regions, as shown in Figure 8f,i, forming three current loops between the top and bottom layers. As a result, the higher resonant frequency of 17.2 GHz is caused by third-order magnetic resonance.<sup>[29]</sup> Therefore, the ultra-wideband absorption response of the proposed MMA originates from the combination of resonance modes excited by magnetic, third-order magnetic and electric resonances.

To verify the simulation results, an MMA prototype was fabricated for experimentation. The structural parameters of the fabrication sample are fixed the same as the simulated model as listed in Table 1. The sample was patterned on an FR-4 substrate with the same properties as in the design using the standard photolithography process. The surface mount resistors with size 0402 and resistance of  $180\ \Omega$  with 1% tolerance were chosen as lumped resistors. A photograph of the fabricated multilayer dielectric MMA sample is shown in Figure 9a, which contains  $15 \times 15$  unit cells (900 resistors) and has an oversize of  $20.4 \times 20.4\ \text{cm}^2$ . The inset photo of Figure 9a shows a fabricated unit cell of the MMA.

The schematic of the test setup for reflection measurement of the fabricated absorber sample is shown in Figure 9b. A vector network analyzer (Rohde and Schwarz ZNB20) together with two

identical linearly polarized standard-gain horn antennas as transmitter and receiver was used to measure the reflection coefficient. Before measuring the sample, the reflection spectrum was calibrated by a copper plate. The distance from antennas to the sample under test (SUT) was about 35 cm. Measurements were taken over a frequency range from 2 to 18 GHz.

Figure 10 shows a comparison of the simulated and measured absorption of the proposed MMA in the case of oblique incidence of  $20^\circ$  for TE and TM polarizations. It should be noted that for our measurement setup as shown in Figure 9b, the minimum oblique incidence is  $20^\circ$  because the antennas cannot be placed too close to each other. We can see a good agreement between experimental and simulation results except for the slightly narrower measured absorption bandwidth of the fabricated MMA under TM polarization. The measured result confirms that the bandwidth with an absorption rate higher than 88% of the MMA entirely covers the C and X bands for both TE and TM polarizations. The measured absorption intensity is slightly poorer than the simulated one due to the imperfection in the SUT fabrication and measurement.

Finally, we compare the absorption performance between the proposed MMA and other wideband MMAs. The performance comparison of the MMAs is conducted in terms of the absorption bandwidth, relative absorption bandwidth, total thickness, and dielectric material, as shown in Table 2. Especially, to evaluate the lightweight properties of the MMAs, we also compare their thickness without airgap (only solid parts are considered). It can be seen that the proposed MMA has the widest RAB among the reported MMAs. Even though the total thickness of the proposed MMA is of a moderate value, the proposed MMA is characterized by the most lightweight design due to the thinnest thickness without an airgap. Moreover, the proposed MMA has the highest RAB per number of lumped resistors, demonstrating that it is the most efficient design with the using of the lumped resistor to broaden the absorption bandwidth.

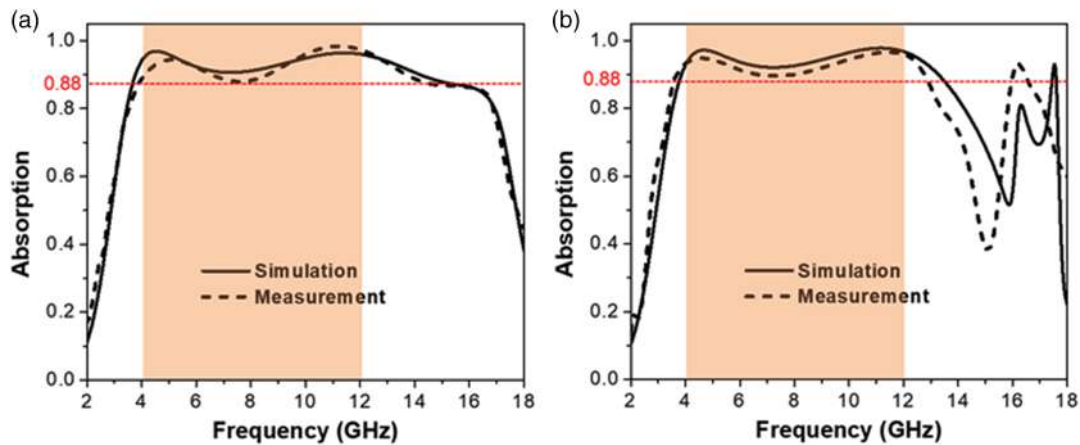


**Figure 10.** Simulated and measured absorption spectra under a) TE polarization and b) TM polarization.

**Table 2.** Comparison of the performance of the proposed MMA and that of other broadband MMAs.

Ref.	Absorption bandwidth <sup>a)</sup> [GHz]	Relative absorption bandwidth <sup>b)</sup> [%]	Relative absorption bandwidth per lumped resistors	Thickness [mm]	Thickness excluding airgap [mm]	Dielectric material
[4]	5–7	33.3	N/A	6.76 (0.113 $\lambda_L$ ) <sup>c)</sup>	6.76 (0.113 $\lambda_L$ )	PVB + glass
[29]	7.8–12.6	47.0	11.75	3.2 (0.083 $\lambda_L$ )	3.2 (0.083 $\lambda_L$ )	FR-4
[35]	4–12	100	N/A	5.2 (0.069 $\lambda_L$ )	3.7 (0.049 $\lambda_L$ )	FR-4 + airgap
[36]	6.79–14.96	75.1	12.5	5.6 (0.127 $\lambda_L$ )	1.6 (0.036 $\lambda_L$ )	FR-4 + airgap
[37]	7.6–18.3	82.6	20.7	3.25 (0.082 $\lambda_L$ )	3.25 (0.082 $\lambda_L$ )	Polyimide + rubber
Our work	3.7–13.6	114.5	28.6	6.4 (0.079 $\lambda_L$ )	1.6 (0.02 $\lambda_L$ )	FR-4 + airgap

<sup>a)</sup>Absorption bandwidth is defined as the frequency band with an absorption above 90%; <sup>b)</sup>Relative absorption bandwidth is defined as the ratio of absorption bandwidth and the center frequency; <sup>c)</sup> $\lambda_L$  is the lowest frequency of an absorption bandwidth.

## 4. Conclusion

An ultra-wideband and lightweight MMA has been proposed to achieve above 90% of absorption in the frequency band of 3.7–13.6 GHz covering the entire C- and X-bands. Moreover, the absorption is un-changed with any change of polarization angle due to its symmetric structure. The contribution of air-gap layer on ultra-wideband absorption property of the designed absorber was first described, and then its absorption mechanism was revealed using the distributions of electric field and surface currents. The measurement of absorption performance of the MMA was conducted to verify the simulation result, indicating the experimental result is consistent with simulation result. Furthermore, the proposed MMA shows an ultra-wide absorption bandwidth with a very lightweight design compared to other reported broadband MMAs, thus the proposed design can be used for both commercial and military applications in C- and X-bands.

## Acknowledgements

This research was supported by Ministry of Education and Training, Vietnam (Grant No. B2021–TDV-05).

## Conflict of Interest

The authors declare no conflict of interest.

## Data Availability Statement

Research data are not shared.

## Keywords

absorbers, broadband, C and X bands, metamaterials, wide-angle

Received: May 3, 2021

Revised: May 29, 2021

Published online:

- [1] B. Zheng, R. Zhang, M. Zhou, W. Zhang, S. Lin, Z. Ni, H. Wang, F. Yu, H. Chen, *Appl. Phys. Lett.* **2014**, *104*, 073502.
- [2] K. P. Kaur, T. Upadhyaya, M. Palandoken, C. Gocen, *Int. J. RF Microw. Comput. Eng.* **2019**, *29*, e21646.
- [3] S. Xie, Z. Ji, L. Zhu, J. Zhang, Y. Cao, J. Chen, R. Liu, J. Wang, *J. Build. Eng.* **2020**, *27*, 100963.

- [4] H. Xiao, Z. Qu, M. Lv, M. Du, W. Zhu, C. Wang, R. Qin, *J. Appl. Phys.* **2019**, *216*, 135107.
- [5] I. Jáuregui-López, P. Rodríguez-Ulbarri, A. Urrutia, S. A. Kuznetsov, M. Beruete, *Phys. Status Solidi RRL* **2018**, *12*, 1800375.
- [6] I. Landy, S. Sajuyigbe, J. J. Mock, D. R. Smith, W. J. Padilla, *Phys. Rev. Lett.* **2008**, *100*, 207402.
- [7] D. J. Gogoi, N. J. Bhattacharyya, *J. Appl. Phys.* **2019**, *124*, 075106
- [8] Q. H. Zhou, S. Zha, L. A. Bian, J. H. Zhang, L. Ding, H. Q. Liu, P. G. Liu, *J. Phys. D: Appl. Phys.* **2019**, *52*, 255102.
- [9] N. Fernez, L. Burgnies, D. Dereudre, D. Lippens, A. Lheurette, *J. Appl. Phys.* **2019**, *125*, 213106.
- [10] M. Zhong, *Opt. Laser Technol.* **2020**, *127*, 106142.
- [11] S. Ji, C. Jiang, J. Zhao, J. Yang, J. Wang, H. Dai, *Curr. Appl. Phys.* **2019**, *19*, 1164.
- [12] T. Q. M. Nguyen, T. K. T. Nguyen, D. T. Le, C. L. Truong, D. L. Vu, T. Q. H. Nguyen, *Plasmonics* **2021**, <https://doi.org/10.1007/s11468-021-01424-7>.
- [13] J. Xu, Y. Fan, X. Su, J. Guo, J. Zhu, Q. Fu, F. Zhang, *Opt. Mater.* **2021**, *113*, 110852.
- [14] F. Yang, Y. Fan, R. Yang, J. Xu, Q. Fu, F. Zhang, Z. Wei, H. Li, *Opt. Express* **2019**, *27*, 25974.
- [15] T. Q. H. Nguyen, T. K. T. Nguyen, T. Q. M. Nguyen, T. N. Cao, H. L. Phan, N. M. Luong, D. T. Le, X. K. Bui, C. L. Truong, D. L. Vu, *Opt. Commun.* **2021**, *468*, 126773.
- [16] J. Lee, Y. J. Yoon, S. Lim, *ETRI J.* **2012**, *34*, 126.
- [17] X. Shen, Y. Yang, Y. Zang, J. Gu, J. Han, W. Zhang, T. J. Cui, *Appl. Phys. Lett.* **2012**, *101*, 154102.
- [18] J. Zhao, S. Wei, C. Wang, K. Chen, B. Zhu, T. Jiang, Y. Feng, *Opt. Express* **2018**, *26*, 8522.
- [19] S. Chen, Y. Fan, F. Yang, Y. Jin, Q. Fu, J. Zheng, F. Zhang, *Phys. Status Solidi RRL* **2019**, *13*, 1900426.
- [20] J. Zhu, Z. Ma, W. Sun, F. Ding, Q. He, L. Zhou, Y. Ma, *Appl. Phys. Lett.* **2014**, *105*, 21102.
- [21] N. T. Q. Hoa, P. D. Tung, P. H. Lam, N. D. Dung, N. H. Quang, *J. Electron. Mater.* **2018**, *47*, 2634.
- [22] D. T. Viet, N. T. Hien, P. V. Tuong, N. Q. Minh, P. T. Trang, L. N. Le, Y. P. Lee, V. D. Lam, *Opt. Commun.* **2014**, *322*, 20.
- [23] V. D. Qui, N. H. Tung, T. V. Huynh, N. D. Dzung, N. T. Binh, V. D. Lam, *Opt. Express* **2018**, *26*, 33253.
- [24] C. Zhang, J. Yang, W. Cao, W. Yuan, J. Ke, L. Yang, T. Cui, *Photonics Res.* **2019**, *7*, 478.
- [25] S. Ghosh, S. Lim, *IEEE Antennas Wirel. Propag. Lett.* **2018**, *17*, 2379.
- [26] J. Xie, S. Quader, F. Xiao, C. He, X. Liang, J. Geng, R. Jin, W. Zhu, I. D. Rukhlenko, *IEEE Antennas Wirel. Propag. Lett.* **2019**, *18*, 536.
- [27] Q. Song, W. Zhang, P. C. Wu, W. Zhu, Z. X. Shen, P. H. J. Chong, Q. X. Liang, Z. C. Yang, Y. L. Hao, H. Cai, H. F. Zhou, Y. Gu, G. Q. Lo, D. P. Tsai, T. Bourouina, Y. Leprince-Wang, A. Q. Liu, *Adv. Optical Mater.* **2017**, *5*, 1601103.
- [28] J. Xie, W. Zhu, I. D. Rukhlenko, F. Xiao, C. He, J. Geng, X. Liang, R. Jin, M. Premaratne, *Opt. Express* **2018**, *26*, 5052.
- [29] T. Q. H. Nguyen, T. K. T. Nguyen, T. N. Cao, H. Nguyen, L. G. Bach, *AIP Adv.* **2020**, *10*, 035326.
- [30] T. T. Nguyen, S. Lim, *Sci. Rep.* **2018**, *8*, 6633.
- [31] F. Costa, A. Monorchio, G. Manara, *IEEE Trans. Antennas Propag.* **2010**, *58*, 1551.
- [32] Z. Yao, S. Xiao, Z. Jiang, L. Yan, B.-Z. Wang, *IEEE Antennas Wirel. Propag. Lett.* **2020**, *19*, 591.
- [33] Y. Shang, Z. Shen, S. Xiao, *IEEE Trans. Antennas Propag.* **2013**, *61*, 6022.
- [34] D. R. Smith, D. C. Vier, T. Koschny, C. M. Soukoulis, *Phys. Rev. E* **2015**, *71*, 036617.
- [35] T. Beeharry, R. Yahiaoui, K. Selemani, H. H. Ouslimani, *Sci. Rep.* **2018**, *8*, 382.
- [36] M. Yoo, S. Lim, *IEEE Trans. Antennas Propag.* **2018**, *71*, 2652.
- [37] H. Chen, X. Yang, S. Wu, D. Zhang, H. Xiao, K. Huang, Z. Zhu, J. Yuan, *Mater. Res. Express* **2018**, *5*, 015804.